AIAA Paper No. 70-553

③

70-553

AIAA PAPER 70-553

CIRCULAR—ARC JET FLAPS AT HYPERSONIC SPEEDS

by
JAMES L. AMICK
University of Michigan
Ann Arbor, Michigan

AIAA Atmospheric Flight Mechanics Conference

TULLAHOMA, TENNESSEE/MAY 13-15, 1970

CIRCULAR-ARC JET FLAPS AT HYPERSONIC SPEEDS*

James L. Amick**
The University of Michigan
Ann Arbor, Michigan

Abstract

Tests at Mach 8 of a forward-inclined two-dimensional jet flap issuing from a slot-nozzle contoured to produce a circular-path jet are compared with theory. Three major regimes of jet strength are observed. Normal-force amplification (based on the jet vacuum normal force) is found to increase with increasing Reynolds number in the weak jet regime, or with decreasing jet strength in the strong jet regime. In all regimes the theory shows that forward inclination of the jet increases normal-force amplification, and over-expansion reduces it. Amplification is predicted by the theory to be almost independent of jet gas properties (stagnation temperature, specific heat ratio, molecular weight) and of the jet Mach number. Agreement between theory and experiment is good in the strong jet regime, where a simple equation with only one empirical constant describes well the experimental results.

Nomenclature

$C_{N_{vac}}$ — normal force coefficient of jet in vacuum
$$= N_{vac}/[(\gamma_1/2) M_1^2 p_1 L]$$

C_{p_b} — base pressure coefficient
$$= (p_b - p_1)/[(\gamma_1/2) M_1^2 p_1]$$

C_{p_2} — plateau pressure coefficient
$$= (p_2 - p_1)/[(\gamma_1/2) M_1^2 p_1]$$

$C_{p_{2_L}}$ — limiting value of plateau pressure coefficient for boundary layer separation near jet (see Eq. (30) or (31)).

K — normal force amplification factor

K' — approximate value of K given by Eq. (35)

K_o — limiting value of K as jet strength approaches zero

K_o' — approximate value of K_o given by Eq. (32)

L — distance from jet to effective origin of boundary layer

M_1 — Mach number of flow ahead of jet with jet off

M_j — Mach number along leading edge of jet

N_I — interaction force per unit span = resultant of jet-induced pressure changes acting on airfoil ahead of jet

N_{vac} — normal force of jet in vacuum, per unit span

$N_{vac_{th}}$ — theoretical value of N_{vac}

p — pressure

p_b — base pressure downstream of jet

p_{o_j} — jet stagnation pressure

p_1 — pressure on flat surface ahead of jet with jet off

p_2 — plateau pressure in separated flow region ahead of jet

R — radius of leading edge of circular-arc jet

Re_L — Reynolds number based on L and flow conditions associated with M_1

Re^* — Reynolds number at throat of slot-nozzle based on w^*

r — radial coordinate

S — distance of separation point ahead of jet

V — velocity

w — width of jet

w^* — throat width of slot-nozzle

α — flow separation angle

β — flow intersection angle between jet and main flow

γ — ratio of specific heats of jet gas

γ_1 — ratio of specific heats of main stream

δ — jet-flap deflection angle (see Fig. 2)

θ — angular coordinate

Introduction

Jets issuing from surfaces exposed to super-sonic flow hold promise as versatile control de-vices, since interaction between a jet and a main flow causes pressure changes on the adjacent sur-face which can result in substantial amplification of the jet reaction force, and since the jet reaction force is always available, even if the density or velocity of the surrounding flow approaches zero.

Theories to describe the jet-interaction pro-cess generally require drastic simplifying assump-tions. However, in the case of a circular-arc jet flap a more rigorous treatment is possible. This results from the simple geometry of the circular-arc jet flap, where the jet sheet emerges from a specially-contoured nozzle and follows concentric circular-arc streamlines in equilibrium with a high-pressure region on its upstream side and a low-pressure region downstream. A typical cir-cular-arc jet flap is shown in the schlieren picture of Fig. 1.
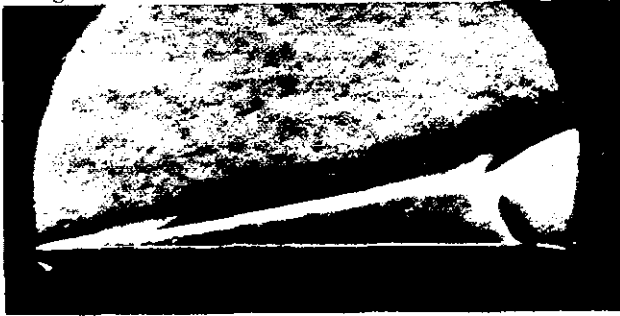
Figure 1.   Schlieren picture of circular-arc jet
flap at $M_1 = 7.5$, $Re_L = 85,000$.

In the hope that knowledge of the interaction mechanism for a special type of jet would also re-veal general principles that apply to other jets, an investigation of the circular-arc jet flap was con-ducted. Theoretical and experimental results of the investigation are presented in this paper.

Circular-Arc Jet-Flap Theory

The flow model considered in this analysis is shown in Fig. 2. Both the jet flow and the main flow are considered to be inviscid, except that the main flow is assumed to separate from the flat sur-face ahead of the jet at an angle α determined by empirical separation equations, and then to join the jet flow at an intersection angle β, which will be left as a variable of the problem, to be evalu-ated by future experiments. The jet nozzle is as-sumed to be so shaped, and the jet stagnation pres-sure so chosen, that the resulting curved jet fol-lows a circular-arc path in equilibrium with the pressure difference $p_2 - p_b$ between the pressure

in the separation region on the upstream side of the jet and the base pressure on the downstream

side. Because the jet is in equilibrium, its width remains constant until the deflected main flow in-tersects with it.
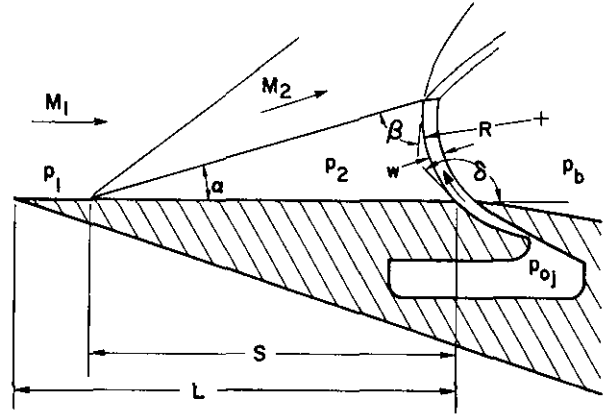
Figure 2.   Circular-arc jet-flap flow model.

Circular Flow Equations

The balance between the radial pressure gra-dient force acting on a fluid element having dimen-sions $r\,d\theta$ and dr, and the centrifugal force acting on the element, can be expressed as

$$r\,d\theta\ dp = r\,d\theta\ dr\,\rho\,V^2/r \qquad (1)$$

For isentropic flow of a perfect gas this equation integrates to

$$(r/R)^2 = \frac{1 - (p_2/p_{o_j})^{(\gamma-1)/\gamma}}{1 - (p/p_{o_j})^{(\gamma-1)/\gamma}} \qquad (2)$$

The jet width is obtained from (2) as

$$w/R = 1 - \left[\frac{1 - (p_2/p_{o_j})^{(\gamma-1)/\gamma}}{1 - (p_b/p_{o_j})^{(\gamma-1)/\gamma}}\right]^{1/2} \qquad (3)$$

The above three equations enable a nozzle to be designed for a circular-arc flow. A typical cir-cular-arc jet-flap nozzle is shown in Fig. 3[1]. This nozzle was designed by the method of charac-teristics, starting at line CH and constructing the initial region of circular-arc flow, CHGL. To this was patched a simple wave region, CGFDEL, upstream of which a source flow was assumed. For this particular nozzle the radius of curvature of the leading streamline ($M_j = 3.07$) is $R = 11.46\,w$.

Normal Force of Jet Alone

The normal force produced by the circular-arc jet-flap alone (that is, when discharging into a vacuum) can be considered in two parts: 1) the

2

force due to pressures acting on all parts of a hypothetical nozzle extending to points A and B in Fig. 3, and 2) the force due to pressure acting on the circular arc BC.
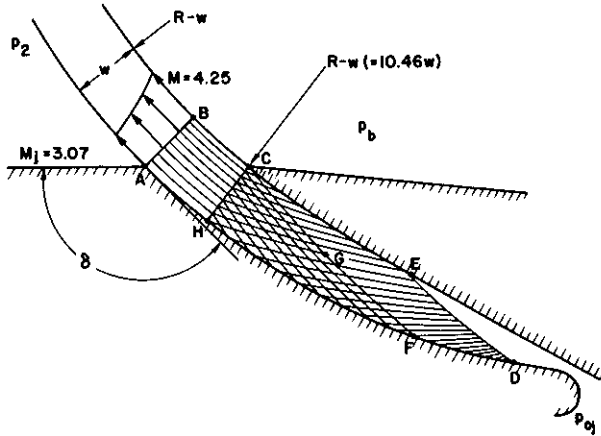

Figure 3. Circular-arc jet-flap nozzle.

The force due to pressures acting upstream of AB acts in a direction opposite that of the jet velocity discharging through AB, and has a magnitude (per unit span) given by the momentum theorem as

$$F = \int_{R-w}^{R} (p + \rho V^2)\, dr \qquad (4)$$

But from Eq. (1)

$$\rho V^2\, dr = r\, dp \qquad (5)$$

so that Eq. (4) becomes

$$F = \int_{R-w}^{R} p\, dr + r\, dp = \int_{p_b(R-w)}^{p_2 R} d(pr)$$

$$= p_2 R - p_b (R - w) \qquad (6)$$

The normal component of this force is

$$N_{AB} = F \sin \delta = [p_2 R - p_b (R - w)] \sin \delta \qquad (7)$$

The circular arc BC is acted on by base pressure. The downward normal component of the force of the jet on BC is

$$N_{BC} = - p_b \Big\{ (R - w) \sin \delta$$

$$- [(R - w)^2 - (R \cos \delta)^2]^{1/2} \Big\} \qquad (8)$$

The normal force of the circular arc jet discharging into a vacuum is the force on the total

hypothetical nozzle, Eq. (7), minus the force on the circular arc BC, Eq. (8).

$$N_{vac} = R \Big\{ p_2 \sin \delta - p_b [(1 - w/R)^2$$

$$- \cos^2 \delta]^{1/2} \Big\} \qquad (9)$$

Interaction Force

The interaction force N_I is defined as the resultant of jet-induced pressure changes acting on the flat plate ahead of the jet. According to this simple model

$$N_I = (p_2 - p_1) S \qquad (10)$$

The separation distance S is related to the jet radius of curvature R as shown in Fig. 2. According to this figure

$$S = R [\cos \beta - \cos (\delta - \alpha)]/\sin \alpha \qquad (11)$$

The flow deflection angle α can be determined from the oblique shock relation

$$\tan \alpha = \frac{P [(M_1^2 - P - 1)/(P + 1)]^{1/2}}{.5 M_1^2 (\gamma_1 + 1) - P} \qquad (12)$$

where

$$P = [(p_2/p_1) - 1] (\gamma_1 + 1)/(2\gamma_1)$$

The interaction force can now be written, by combining Eq. (10) and (11), as

$$N_I = (p_2 - p_1) R [\cos \beta - \cos (\delta - \alpha)]/\sin \alpha \qquad (13)$$

Amplification Factor

A normal-force amplification factor can be defined as the ratio of the normal force due to the jet (including interaction effects) to the normal force of the jet discharging into a vacuum, that is

$$K = [N_I + N_{vac} - p_1 w']/N_{vac} \qquad (14)$$

where w' is the chordwise extent of the jet slot, which can be evaluated from Fig. 3 as the length AC:

$$w' = R \sin \delta - [(R - w)^2 - (R \cos \delta)^2]^{1/2} \qquad (15)$$

Equations (9), (13), and (15) inserted in Eq. (14) yield

$$K = \frac{(p_1 - p_b) W + (p_2 - p_1)\left(\dfrac{\cos \beta}{\sin \alpha} - \dfrac{\cos \delta}{\tan \alpha}\right)}{p_2 \sin \delta - p_b W} \qquad (16)$$

3

where

$$W \equiv \left[(1 - w/R)^2 - \cos^2 \delta \right]^{1/2}$$

From Eq. (16) and the preceding Eq. (3) and (12) it can be seen that the amplification factor K is a function of p_2/p_1, p_b/p_1, p_2/p_{0j}, β, δ, M_1, γ, and γ_1. Amplification factor is independent of jet stagnation temperature or molecular weight.

Jet Vacuum Normal-Force Coefficient

A useful parameter for correlating the amplification factor of a jet flap is the coefficient of the jet vacuum normal-force, defined as

$$C_{N_{vac}} = N_{vac}/[(\gamma_1/2) M_1^2 p_1 L] \qquad (17)$$

where L is the distance from the leading edge to the jet slot. This parameter is a measure of the jet strength in relation to that of the main stream.

Equation (17) can be expressed in terms of p_2/p_1 by substituting into it Eq. (19) and (11):

$$C_{N_{vac}} = \frac{(p_2 \sin \delta - p_b W)(\sin \alpha) S/L}{(\gamma_1/2) M_1^2 p_1 [\cos \beta - \cos (\delta - \alpha)]} \qquad (18)$$

The separation location S/L is a function of p_2/p_1, as given by semi-empirical plateau pressure equations. Thus, for pure laminar separation[2]

$$p_2/p_1 = 1 + 1.27 \left\{ M_1^3 / [Re_L (L - S)/L]^{1/2} \right\}^{1/2} \qquad (19)$$

where L is the distance from the flat plate leading edge (or equivalent origin of the boundary layer) to the leading edge of the jet slot; and Re_L is Reynolds number based on L and the conditions associated with p_1 and M_1. Similarly, for turbulent separation, the plateau pressure (or first peak pressure) can be approximated by[3]

$$p_2/p_1 = 1 + \frac{2.6 (M_1^2 - 1)^{1/2}}{[Re_L (L - S)/L]^{1/10}} \qquad (20)$$

Equations (19) and (20) can be solved for S/L to give, for laminar separation

$$S/L = 1 - 2.60 M_1^6 / \left\{ Re_L [(p_2/p_1) - 1]^4 \right\} \qquad (21)$$

and, for turbulent separation

$$S/L = 1 - 14,100 (M_1^2 - 1)^5 / \left\{ Re_L [(p_2/p_1) - 1]^{10} \right\} \qquad (22)$$

The variation of amplification factor K with jet normal force coefficient $C_{N_{vac}}$ is defined implicitly by Eq. (16) and (18) with the help of

Eq. (3), (12), and (21) or (22). In all of these equations p_2/p_1 is a parameter, so that calculation of points defining the relationship of K to $C_{N_{vac}}$ begins with an assumed value of p_2/p_1. Fixed, but arbitrary, values of β and p_b/p_1 must also be chosen, based, if possible, on empirical considerations. (However, the effects of these two empirical constants on the results are not very great.)

Typical results of the circular-arc jet-flap theory are shown in Fig. 4, along with a strong-jet approximation discussed later. (In this and the following figures the type of separation is laminar, $M_1 = 8$, $p_b = .3 p_1$, and $\gamma = \gamma_1 = 1.4$, unless otherwise noted.) The main features of the relation between K and $C_{N_{vac}}$ are 1) the amplification factor approaches a finite limit for a weak jet, and 2) the amplification factor decreases monotonically as jet strength increases, approaching a value of unity for infinite jet strength relative to the main stream.
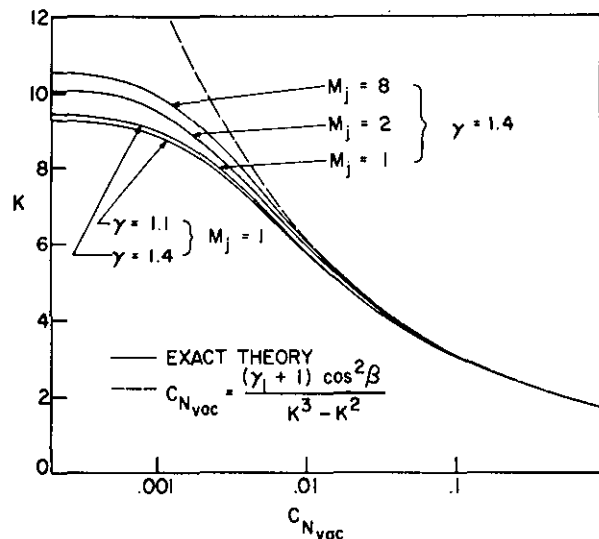
Figure 4. Normal-force amplification factor vs. jet vacuum normal-force coefficient, for circular-arc jet flaps at design conditions. $\delta = 90°$, $Re_L = 10^7$, $\beta = 25°$.

It should be noted that Fig. 4 does not represent the performance of any given slot-nozzle as jet stagnation pressure ratio is varied, but rather, it represents a series of design conditions which vary in $C_{N_{vac}}$ through variation in the relative size of the slot-nozzle, with the effective expansion ratio p_{0j}/p_2 always kept constant at the design value.

Mass Flow and Specific Impulse

The mass flow rate of the circular-arc jet flap can be obtained by integrating across the jet. This integration is carried out in Ref. 4, and an infinite series is obtained which can usually be evaluated

4

accurately with just a few terms. Various kinds of specific impulse are also derived in Ref. 4.

Hypersonic Approximations

For hypersonic flow, the oblique shock relation of Eq. (12) reduces to

$$\tan \alpha = \frac{(p_2/p_1) - 1}{M_1 \left\{ \frac{\gamma_1 (\gamma_1 + 1)}{2} \left[\frac{p_2}{p_1} + \frac{\gamma_1 - 1}{\gamma_1 + 1} \right] \right\}^{1/2}} \quad (23)$$

Neglecting w/R, which is often small compared with unity, and letting $\sin \alpha = \tan \alpha$ and $\cos \alpha = 1$, Eq. (16) and (23) combine to give

$$K = \left\{ [(\cos \beta - \cos \delta)/\sin \delta][(\gamma_1 + 1) C_{p_2} + 4/M_1^2]^{1/2} - C_{p_b} \right\} / (C_{p_2} - C_{p_b}) \quad (24)$$

where

$$C_{p_2} = (p_2 - p_1)/[(\gamma_1/2) p_1 M_1^2]$$

and

$$C_{p_2} = (p_b - p_1)/[(\gamma_1/2) p_1 M_1^2]$$

Strong-Jet Approximation

For strong jets (those causing separation of the boundary layer near the leading edge) $S/L \cong 1$, and p_1 and p_b can be neglected in comparison to p_2, so that Eq. (24) and (18) become

$$K = \left\{ (\cos \beta - \cos \delta)[(\gamma_1 + 1) C_{p_2}]^{1/2} \right\} / (C_{p_2} \sin \delta) \quad (25)$$

$$C_{N_{vac}} = (C_{p_2} \sin \alpha \sin \delta)/[\cos \beta - \cos (\delta - \alpha)] \quad (26)$$

These approximations, when applied to Eq. (16), give

$$K = (\cos \beta - \cos \delta \cos \alpha)/(\sin \alpha \sin \delta) \quad (27)$$

so that Eq. (26) becomes

$$C_{N_{vac}} = C_{p_2}/(K - 1) \quad (28)$$

Then Eq. (25), squared, gives

$$C_{N_{vac}} = \frac{(\gamma_1 + 1)}{(K - 1)} \left[\frac{\cos \beta - \cos \delta}{K \sin \delta} \right]^2 \quad (29)$$

From Eq. (29) it appears that appropriate correlation parameters for strong-jet results are K and $C_{N_{vac}} \sin^2 \delta/(\cos \beta - \cos \delta)^2$. A plot using these parameters as coordinates is shown in Fig. 5. (Figure 4 is a similar plot for the special case
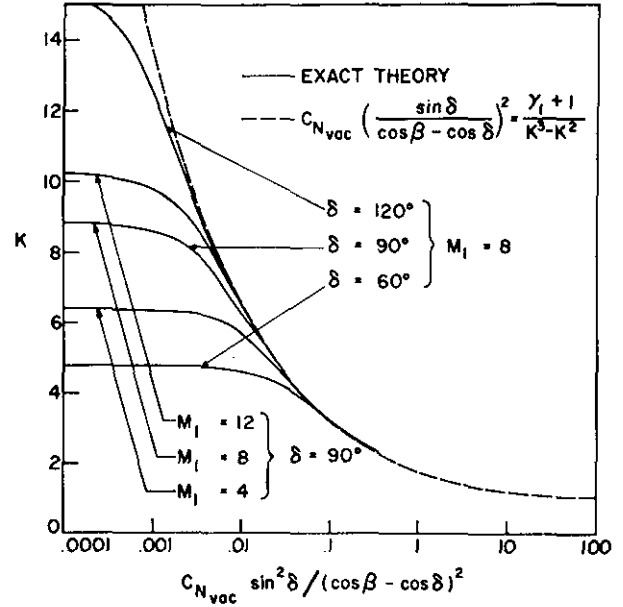

Figure 5. Effects of jet-flap deflection angle and free stream Mach number. $Re_L = 10^6$, $M_j = 8$, $\beta = 25°$.

of $\delta = 90°$.) It can be seen that there is good agreement between the exact theory and the strong-jet approximation, for sufficiently strong jets.

Weak-Jet Approximation

Limiting values of amplification factor (designated K_0) are approached as jet strength decreases, as can be seen in Fig. 4 and 5. In the weak-jet limit, boundary layer separation occurs near the jet. Thus, a limiting value of the plateau pressure coefficient $C_{p_{2_L}}$ may be calculated from simplified forms of Eq. (19) or (20) as

$$C_{p_{2_L}} = (2.54)/\gamma_1)/\left[M_1 (Re_L)^{1/2}\right]^{1/2} \quad (30)$$

for laminar separation, or

$$C_{p_{2_L}} = 5.2 [(M_1^2 - 1)^{1/2}/(Re_L)^{1/10}]/(\gamma_1 M_1^2) \quad (31)$$

for turbulent separation. An approximate value of the limiting amplification factor is obtained by substituting $C_{p_{2_L}}$ for C_{p_2} in Eq. (24):

$$K_0' = \left\{ [(\cos \beta - \cos \delta)/\sin \delta][(\gamma_1 + 1) C_{p_{2_L}} + 4/M_1^2]^{1/2} - C_{p_b} \right\} / (C_{p_{2_L}} - C_{p_b}) \quad (32)$$

5

The limiting amplification factor is shown by the above approximate equation to be independent of γ and M_j. The approximate equation is very accurate for M_1 values of 4 or more, the maximum discrepancy being only about 2% over a wide range of conditions, excluding δ values less than 90°.

General Correlation

It has been found that the strong-jet approximation

$$K^3 - K^2 = [(\cos \beta - \cos \delta)/\sin \delta]^2 (\gamma_1 + 1)/C_{N_{vac}} \qquad (33)$$

can be generalized to apply to all jet strengths as follows:

$$\frac{(K')^3 - (K')^2}{K_0^3 - K_0^2} = 2A \left[1 - \frac{(K')^3 - (K')^2}{K_0^3 - K_0^2} \right]^{1/2} \qquad (34)$$

where K' designates the approximate value of K defined by this equation, as distinguished from the value of K given by the exact theory, and

$$A \equiv \frac{\gamma_1 + 1}{(K_0 - 1) \, 2C_{N_{vac}}} \left(\frac{\cos \beta - \cos \delta}{K_0 \sin \delta} \right)^2$$

Equation (34) can be solved to give

$$K' = (B + C)^{1/3} + (B - C)^{1/3} + 1/3 \qquad (35)$$

where

$$B \equiv (K_0^3 - K_0^2) \, A \left[(A^2 + 1)^{1/2} - A \right] + 1/27$$

and

$$C \equiv (B^2 - 1/729)^{1/2}$$

Two general parameters are involved in Eq. (34). One of these, an amplification factor parameter, is the quantity $[(K')^3 - (K')^2]/(K_0^3 - K_0^2)$; the other is a jet force parameter:

$$C_{N_{vac}} (K_0 - 1)[K_0 \sin \delta/(\cos \beta - \cos \delta)]^2 .$$

These two parameters correlate the circular-arc jet-flap theoretical results; they are therefore suggested as possible correlating parameters for experimental results.

The asymptotic behavior of Eq. (35) is correct; that is, for very weak jets K' approaches K_0, and for infinitely strong jets K' approaches unity, as it should. For intermediate jet strengths errors are less than 12% for a wide range of parameters.

Flow Regimes

Three distinct flow regimes can be distinguished in Fig. 4 and 5: 1) a weak-jet regime, where separation occurs near the jet (typified by an almost constant K as $C_{N_{vac}}$ decreases), 2) a strong-jet regime, where separation occurs near the leading edge (recognized in Fig. 4 and 5 by a close approach to the strong-jet approximation of Eq. (29)), and 3) an intermediate-jet regime, between the weak-jet and strong-jet regimes. The boundaries between these regimes are somewhat arbitrary, and fall at different $C_{N_{vac}}$ values for different configurations.

In the weak-jet regime the amplification factor is not directly dependent on jet strength ($C_{N_{vac}}$) but may vary with p_{oj}/p_1 as will be shown later. It is assumed that in this regime the separation point is so close to the jet that the separation region pressure p_2, which is a function of the local Reynolds number at separation, remains constant as jet strength is varied. Under these conditions, doubling the jet width, for instance, causes a doubling of the area of the interaction field, with the pressure at corresponding points remaining constant, so that the interaction force varies directly as the jet vacuum force, and amplification therefore remains constant.

In the intermediate-jet regime, amplification decreases with increasing jet strength. As the jet strength increases, the separation point moves forward, causing the separation region pressure to increase because of the reduction in Reynolds number at separation (assuming constant Re_L). This increase in the separation region pressure causes a reduction in effective penetration height of the jet from what it would have been if the separation region pressure had remained constant. Consequently, the percentage increase in interaction force is less than that in jet vacuum force, resulting in a decrease in amplification level.

In the strong-jet regime, amplification is independent of Reynolds number, since the separation point is near the leading edge. Amplification continues to decrease with increasing jet strength as in the intermediate-jet regime, since the separation region pressure still increases with jet strength.

In each flow regime there are only a few important parameters. In the weak-jet regime, free stream Mach number M_1 and jet deflection angle δ are the main parameters that control the level of amplification. In addition, for a laminar boundary layer the Reynolds number Re_L has an important influence. Amplification increases with increasing

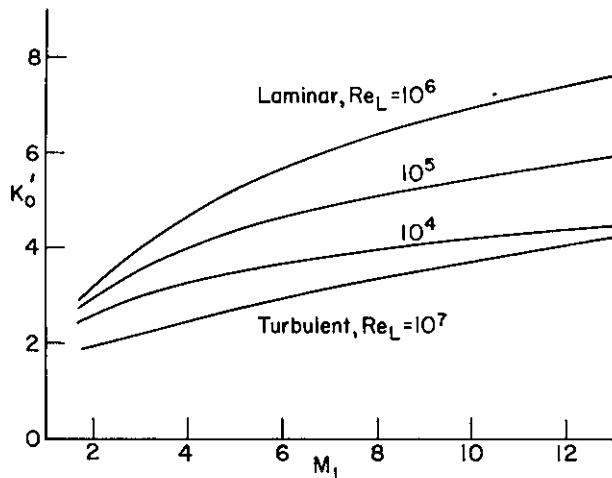values of all of these parameters, as illustrated in Fig. 6 and 7.

Figure 6. Approximate normal-force amplification factor in weak-jet regime, normal jet ($\delta = 90^\circ$). $\beta = 50^\circ$.
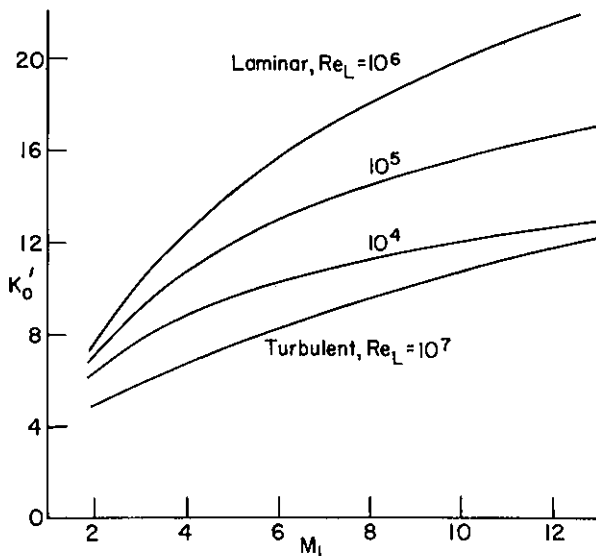

Figure 7. Approximate normal-force amplification factor in weak-jet regime, forward-inclined jet ($\delta = 135^\circ$), $\beta = 50^\circ$.

In the strong-jet regime the important parameters are δ and $C_{N_{vac}}$. Amplification increases with δ and decreases with increasing $C_{N_{vac}}$, as shown in Fig. 8.

In the intermediate-jet regime there occurs a gradual shift in importance between the weak-jet parameters and the strong-jet parameters.
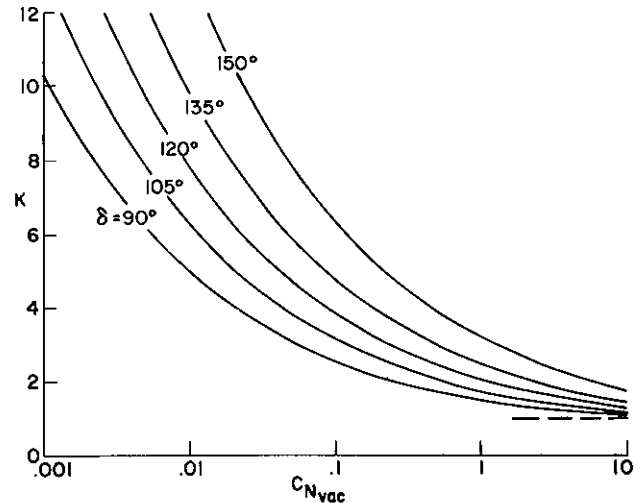

Figure 8. Effect of jet-flap deflection angle in the strong-jet regime, by Eq. (29). $\beta = 50^\circ$.

Constant-Throat-Width Theory

The preceding theoretical development was based on a constant effective jet pressure ratio p_{oj}/p_2, with jet strength varied by changing the slot-nozzle size. A much more complex situation arises when attempting to describe the performance of a given sized nozzle with varying jet pressure ratio, since departures from the design pressure ratio result in a jet flow that is either underexpanded or overexpanded.

A first order approximation to the off-design flow can be made by replacing the complex pattern of shocks and expansion waves of the actual under- or overexpanded flow with a hypothetical circular-arc jet flow attached to the downstream lip of the slot nozzle, its shape fixed by the requirements that it have the same critical area (throat width) as the actual nozzle and that it be in equilibrium, following isentropic expansion, with the pressures p_2 and p_b on its upstream and downstream faces. Results of this constant-throat-width theory for a particular case are shown in Fig. 9. (Here it is assumed that the nozzle throat width ratio w^*/L is less than 4×10^{-9}, so that even for the highest jet pressure ratio shown the interaction is in the weak jet regime.) While the effect of underexpansion is relatively small, overexpansion can cause a severe loss in normal-force amplification.

Other results of this approximate theory are shown in Fig. 10 for larger throat-width ratios. Although this theory represents a drastic simplification of reality, it does give results which approach smoothly the proper limits for very weak and for very strong jets. Thus, on the weak-jet
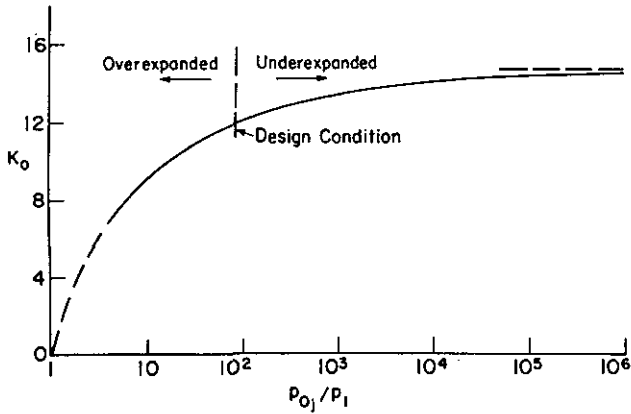
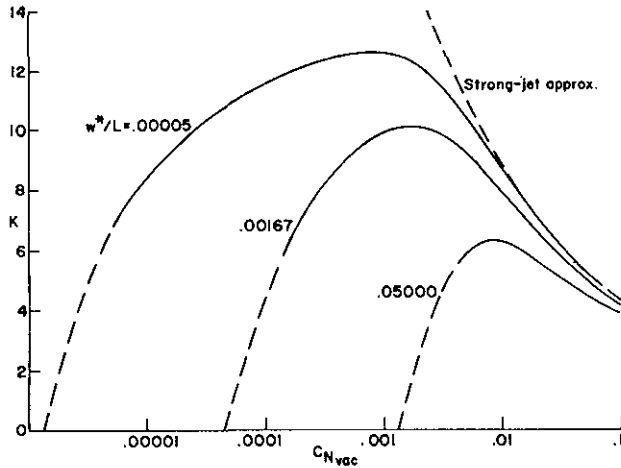Figure 9. Effect of jet pressure ratio in the weak-jet regime. $Re_L = 500,000$, $\delta = 135^O$, $\beta = 75^O$.

Figure 10. Effect of jet throat width. $M_1 = 7.9$, $Re_L = 750,000$, $\delta = 135^O$, $\beta = 65^O$, $p_b = 0$. Design value of $M_j = 3.07$.

end it approaches $K = 0$ at $p_{oj}/p_1 = 1$, while for strong jets it approaches the strong-jet approximation.

Some of these theoretical trends are compared with experimental results in the next section.

Experiment

Circular-arc jet-flap tests at Mach 8 were conducted in the 6.6-inch-diameter hypersonic wind tunnel at The University of Michigan. The model consisted of a 3-inch-square flat plate, at the trailing edge of which was a contoured slot nozzle designed to produce a circular-arc jet flap with a deflection angle of $\delta = 135^O$ (jet inclined 45° forward of the normal to the flat plate). The model

was mounted on a hollow sting instrumented with strain gages to measure normal force and moment.

The circular-arc jet-flap model is shown in Fig. 11, with one endplate removed to reveal the jet air stagnation chamber and the slot-nozzle shape. The contour of the slot nozzle followed approximately the design of Fig. 3, with a boundary-layer allowance added[5]. The nominal throat width was .005 inch. The rearward-sloping surface behind the slot is believed to have had negligible effect on the normal force, with the jet either on or off.
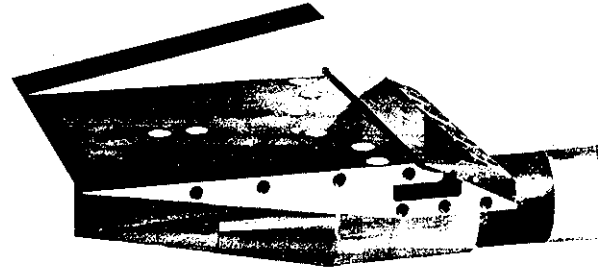

Figure 11. Circular-arc jet-flap model with endplate removed to show cross section of slot-nozzle and jet stagnation chamber.

Several sets of endplates were used with the model to approximate two-dimensional flow. Wedge endplates (one of which is shown in Fig. 11) were used in the strong jet regime, with the wedge angle chosen so that the upper surfaces of the wedges were approximately coincident with the plane of the separated shear layer when the jet was operating. Thus, the inner vertical sides of the wedges were exposed only to the separated flow; consequently, there was no side-wall boundary layer to be separated by the separation shock near the leading edge, in contrast to the troublesome boundary layer problems which may arise with conventional endplates.

For weaker jets, partial-chord endplates were used. Along with these endplates the model was also equipped with lower endplates that had flat outer surfaces and supersonic leading edges. Thus, high pressures from the beveled lower surface of the model could not propagate onto the flat plate ahead of the leading edges of the partial-chord endplates. The reason for using partial- rather than full-chord endplates was to reduce the length Reynolds number of the boundary layers on the endplates, so that they would not be separated by the oblique shock accompanying boundary-layer separation on the flat plate. These endplates had a chordwise adjustment, so that they could be positioned with their leading edges close to the separation point of the boundary layer on the flat plate.

In order to measure amplification factor it is necessary to know the jet vacuum normal force.

8

For this purpose the normal force of the jet discharging into the evacuated tunnel was measured. These measurements were corrected to vacuum conditions by adding the product of the ambient pressure and the projected exit area of the jet. Results of these measurements are shown in Fig. 12 as ratios (N_{vac}/N_{vacth}) of the measured jet normal force in a vacuum to the theoretical value, plotted against $(Re^*)^{-.5}$, the inverse root of the slot-nozzle throat Reynolds number. (For this nozzle $N_{vacth} = 1.165\, p_{oj}\, w^*$, compared with $1.268\, p_{oj}\, w^*$ for a sonic, normal jet.) For throat Reynolds numbers smaller than 1300 the data fall on a straight line through $N_{vac} = N_{vacth}$ at $Re^* = \infty$, as would be expected with a laminar boundary layer. For higher Reynolds numbers, the vacuum normal force falls below the straight line, possibly indicating transition to turbulence.
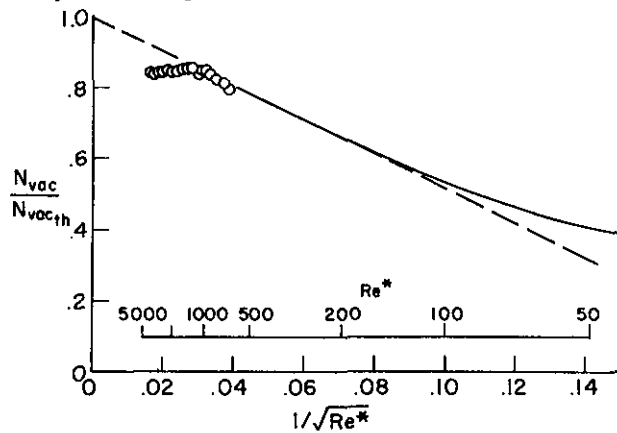

Figure 12. Jet vacuum normal force vs. slot-nozzle throat Reynolds number.

The solid curve shown in Fig. 12 was used to obtain values of the jet vacuum normal force for throat Reynolds numbers in the range 50-600. No measured values were obtained in this range because of difficulty in evacuating the tunnel to less than 2.8 torr, and because the jet stagnation pressure had to be at least 100 times the tunnel pressure to avoid induced flow effects. The curve shown was chosen to give a smooth approach to $N_{vac}/N_{vacth} = 0$ at $Re^* = 0$.

The main results of the tests are shown in the amplification vs. jet strength plot of Fig. 13. Here the experimental results are compared with theoretical curves calculated by the constant-throat-width theory and by the strong-jet approximation. For the constant-throat-width theory, β values were chosen to fit the strong-jet data for each of the two cases, and p_b was chosen as zero to minimize the difference between theoretical and experimental maximum K values.

Since the jet flow for the highest values of CN_{vac} of Fig. 13 is far from the design condition (estimated at about $CN_{vac} = .008$) and therefore much different from the constant-thickness
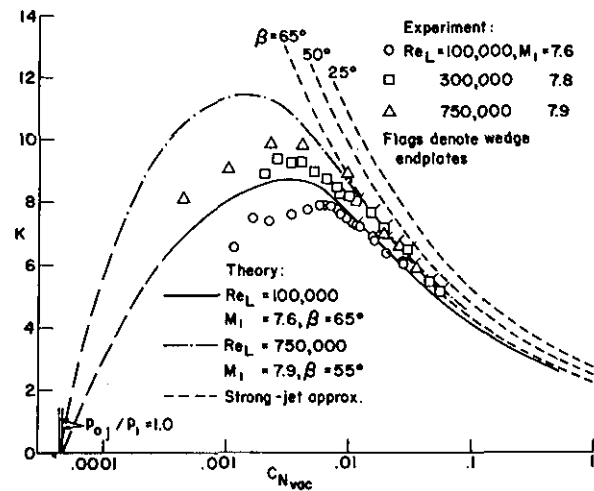

Figure 13. Comparison of theory and experiment.

circular-arc jet assumed in deriving the strong-jet approximation, it can be concluded from the good agreement between theory and experiment that Eq. (29), representing the strong-jet approximation, is an expression of a more general principle applying also to underexpanded jets. Indeed, tests of a sonic, normal jet flap[6] also showed good agreement with the strong-jet approximation, although the indicated β value was somewhat lower ($\sim 50^\circ$).

Conclusions

A theory has been developed for the two-dimensional interaction between a supersonic main stream and a jet flap that follows a circular-arc path. From this theory, the following conclusions, expected to apply also to other types of jet flaps, can be drawn:

1. The normal force amplification factor is a strong function of the jet-flap deflection angle. Increasing this angle from 90° to 135° causes a doubling of the normal force due to the jet in some cases.

2. Effects of jet pressure ratio are small except when off-design operation produces overexpanded nozzle flow, which may result in large reductions in amplification factor.

3. In the weak-jet regime, amplification increases with free stream Mach number and, for a laminar boundary layer, with increasing Reynolds number.

4. In the strong-jet regime, amplification decreases with increasing jet vacuum normal-force coefficient.

5. Jet Mach number and specific heat ratio have little effect on amplification factor. Amplification is independent of jet stagnation temperature or molecular weight.

9

Experimental results for a forward-inclined
($\delta = 135^{\circ}$) circular-arc jet-flap at Mach 8 confirm
the predicted Reynolds number and jet pressure
ratio effects, and show good agreement, for large
jet strengths, with the strong-jet approximation
(Eq. (29)), when a suitable value of the empirical
constant β is chosen.

References

1. Amick, J. L., "Circular-Arc Jet-Flap Noz-
    zles," Section III/4a, Research and Develop-
    ment Programs Quarterly Report, January-
    March 1968 APL/JHU U-RQR/68-1, April
    1968, Applied Physics Laboratory, The Johns
    Hopkins University.

2. Amick, J. L., "A Semiempirical Relation for
    Laminar Separation," Journal of the Aero/
    Space Sciences, Vol. 26, No. 9, September
    1959, p. 603.

3. Amick, J. L. and Carvalho, G. F., "Interac-
    tion Effects of a Jet Flap on a 60° Delta Wing
    at Mach Number 4, and Comparison with
    Two-Dimensional Theory," APL/JHU CM
    1031, February 1963, Department of Aero-
    space Engineering, The University of Michi-
    gan.

4. Amick, J. L., "Circular-Arc Jet Flaps at
    Supersonic Speeds — Two-Dimensional
    Theory," APL/JHU CR-24, July 1966, De-
    partment of Aerospace Engineering, The Uni-
    versity of Michigan.

5. Amick, J. L., "Circular-Arc Jet Flap Inter-
    action at Mach 8," Section III/3b, Research
    and Development Programs Quarterly Report,
    January-March 1969, APL/JHU U-RQR/69-1,
    April 1969, Applied Physics Laboratory, The
    Johns Hopkins University.

6. Amick, J. L., "Hypersonic Tests of Control
    Jets," Section III/6b, Research and Develop-
    ment Programs Quarterly Report, October-
    December 1967, APL/JHU U-RQR/67-4,
    January 1968, Applied Physics Laboratory,
    The Johns Hopkins University.